Progress in Biophysics and Molecular Biology 160 (2021) 43–52

Contents lists available at ScienceDirect

Progress in Biophysics and Molecular Biology

journal homepage: www.elsevier.com/locate/pbiomolbio

Original Research

Localized reconstruction in Scipion expedites the analysis of symmetry mismatches in cryo-EM data

Vahid Abrishami [a, b], Serban L. Ilca [c], Josue Gomez-Blanco [d, e], Ilona Rissanen [a, b], José Miguel de la Rosa-Trevín [f], Vijay S. Reddy [g], José-Maria Carazo [d], Juha T. Huiskonen [a, b, c, *]

[a] Institute of Biotechnology, Helsinki Institute of Life Science HiLIFE, University of Helsinki, 00014, Helsinki, Finland
[b] Molecular and Integrative Biosciences Research Programme, Faculty of Biological and Environmental and Sciences, University of Helsinki, 00014, Helsinki, Finland
[c] Division of Structural Biology, Wellcome Centre for Human Genetics, University of Oxford, Roosevelt Drive, Oxford, OX3 7BN, UK
[d] Biocomputing Unit, National Center for Biotechnology (CSIC), Calle Darwin 3, Campus Universidad Autónoma de Madrid, Cantoblanco, 28049, Madrid, Spain
[e] Current address: Department of Anatomy & Cell Biology, McGill University, 3640 University Street, Montreal, Quebec, H3A 0C7, Canada
[f] Department of Biochemistry and Biophysics, Science for Life Laboratory, Stockholm University, Stockholm, Sweden
[g] Department of Integrative Structural and Computational Biology, The Scripps Research Institute, North Torrey Pines Road, La Jolla, 92037, CA, USA

ARTICLE INFO

Article history:
Received 1 February 2020
Received in revised form
14 May 2020
Accepted 16 May 2020
Available online 26 May 2020

Keywords:
Cryo-EM
Single-particle analysis
Asymmetric reconstruction
Symmetry mismatch
Symmetry relaxation
Localized reconstruction

ABSTRACT

Technological advances in transmission electron microscopes and detectors have turned cryogenic electron microscopy (cryo-EM) into an essential tool for structural biology. A commonly used cryo-EM data analysis method, single particle analysis, averages hundreds of thousands of low-dose images of individual macromolecular complexes to determine a density map of the complex. The presence of symmetry in the complex is beneficial since each projection image can be assigned to multiple views of the complex. However, data processing that applies symmetry can average out asymmetric features and consequently data analysis methods are required to resolve asymmetric structural features. Scipion is a cryo-EM image processing framework that integrates functions from different image processing packages as plugins. To extend its functionality for handling symmetry mismatches, we present here a Scipion plugin termed LocalRec implementing the localized reconstruction method. When tested on an adenovirus data set, the plugin enables resolving the symmetry-mismatched trimeric fibre bound to the five-fold vertices of the capsid. Furthermore, it improves the structure determination of the icosahedral capsid by dealing with the defocus gradient across the particle. LocalRec is expected to be widely applicable in a range of cryo-EM investigations of flexible and symmetry mismatched complexes.

1. Introduction

Cryogenic electron microscopy (cryo-EM) is a powerful technique of structural biology. When combined with single particle analysis (SPA), it facilitates the study of biological macromolecules and their complexes by yielding three-dimensional (3D) reconstructions, which are 3D maps of the macromolecular electrostatic potential (referred to here as density maps). If the resolution of the density map is sufficient, typically better than 4.0 Å, it is possible to derive an atomic model of the complex to gain insights into its function. Because cryo-EM images suffer from low signal-to-noise ratio, in order to reach sufficient signal at the target resolution tens or hundreds of thousands of images of the target protein or complex (so-called 'particles') are required. The required number of particles is reduced by the presence of symmetry in the complex as each individual particle effectively contributes several symmetry-related views of the complex. However, when symmetry is utilized in calculating the density map, features that do not follow the assumed symmetry are incorrectly averaged. Conversely, if the assumption of a certain symmetry is only an approximation, it may reduce the attainable resolution of the whole complex.

To handle symmetry mismatches, several approaches have been

* Corresponding author. Institute of Biotechnology, Helsinki Institute of Life Science HiLIFE, University of Helsinki, 00014, Helsinki, Finland.
E-mail address: juha.huiskonen@helsinki.fi (J.T. Huiskonen).

https://doi.org/10.1016/j.pbiomolbio.2020.05.004

developed (Huiskonen, 2018; Goetschius et al., 2019). These include standard asymmetric refinement (SAR) (Guo et al., 2013) and symmetry relaxation (Morais et al., 2001) in addition to symmetry expansion, focused classification (Scheres, 2016; Grigorieff, 2016) and multibody refinement (Nakane et al., 2018). The SAR approach handles symmetry mismatches simply by ignoring any symmetry in the complex. This method is computationally expensive since it searches for orientation parameters over the full angular space, and the signal from the dominant symmetry can bias these orientation parameters. Assuming that the asymmetric substructure is locked into the complex, the performance of SAR can be improved using the symmetry relaxation technique. This approach uses the alignment information from a previous refinement run using the dominant symmetry and limits the search space to *n* discrete orientations related to the "symmetry mates" of the particle (e.g. 60 symmetry mates in the case of icosahedral symmetry). Although this method is efficient and less likely to get trapped in a local minimum, it is limited to structures with a single symmetry-mismatched subunit. To overcome this limitation, the combination of symmetry expansion and focused classification/refinement can be used for structures with more than one symmetry-mismatched substructure. This approach treats asymmetric units or smaller subunits of the complex as if they were individual particles, by expanding symmetry to generate all symmetry-related orientation parameters for each particle. A mask defining a single subunit is then applied on the volumes during classification and/or refinement and this way each subunit is analysed independently from other subunits. Even though this method has been widely used for asymmetric reconstruction, expanding symmetry increases the number of particles by a factor of symmetry order (e.g. 60 for icosahedral symmetry) which can be computationally expensive for large complexes such as viruses. Additionally, the center of mass of the subunit should be moved to the centre of the subunit for proper local alignment.

To overcome some of the limitations of earlier methods for handling symmetry mismatches, we have previously published a method called localized reconstruction (Ilca et al., 2015). In this method, smaller image areas (sub-particles), corresponding to different symmetry-related subunits, are extracted from particle images and then processed as if they were individual particles. The orientation of each sub-particle is calculated using the orientation and symmetry of the original particle. Furthermore, if the sub-particle is symmetric itself, it can be aligned to its own symmetry convention. As the sub-particles are located at different heights in the original particle, their defocus value is adjusted accordingly. In contrast to the "expand symmetry and focused classification/refinement approach", localized reconstruction requires less memory as the sub-particles can be considerably smaller than the original particle. The original implementation of localized reconstruction, however, offered no graphical user interface and was linked to a single specific software, limiting its wider applicability.

Here, to increase the accessibility of the localized reconstruction method, we have integrated the method as a plugin called LocalRec to the Scipion software framework (de la Rosa-Trevín et al., 2016). The Scipion framework integrates different protocols from several well-established SPA packages, including those handling symmetry-mismatches (Table 1). Using the Scipion LocalRec plugin, one can define and extract sub-particles, and follow conventional SPA workflows using a range of state-of-the-art methods in order to resolve the symmetry-mismatched subunit. In addition, we introduce a new protocol for creating a composite map of the particle from several subunit reconstructions, similar to the 'block-based' reconstruction method (Zhu et al., 2018). We demonstrate different functions of the plugin by improving the resolution of the adenovirus subunits after tackling their inherent flexibility and/or associated symmetry-mismatches. In general, LocalRec plugin is expected to increase the applicability of the localized reconstruction method and to ease its integration with other methods *via* its incorporation into Scipion.

2. Materials and methods

2.1. Icosahedral reconstruction of adenovirus

To test the developed Scipion protocols, we used a dataset of 1326 cryo-EM micrographs of human adenovirus subspecies D serotype 26 (HAdV-D26) that has been published earlier (Yu et al., 2017). The micrographs (pixel size 1.31 Å), 8684 particle coordinates and a 3D reconstruction of the particle (EMD-8471) were imported using *scipion - import micrographs*, *scipion - import coordinates* and *scipion - import volumes* protocols, respectively. Contrast transfer function (CTF) parameters were estimated using protocol *grigoriefflab - ctffind4* (Rohou and Grigorieff, 2015). The remaining processing steps were performed using RELION 3.0.7 and associated Scipion protocols. Particles were extracted from micrographs using *relion - particles extraction* using both the original sampling (particle box size 1200 × 1200 pixels) and a down-sampling factor of 3 (box size 400 × 400 pixels). The down-sampled particles were refined using *relion - 3D auto-refine* to determine their alignment parameters (origins and orientations in icosahedral I1 convention). The 3D reconstruction of the particle was low-pass filtered to 40 Å to serve as an initial model. The resolution of this initial refinement using the down-sampled particles (7.9 Å) was limited by the Nyquist frequency. The alignment parameters from the down-sampled particles were assigned to the original particles using *scipion - alignment assign* protocol for high-resolution reconstruction. This was performed using *relion - 3D auto-refine*. For computational efficiency, orientation and origin search was skipped by limiting the alignment to one orientation and translation. Protocol *relion - post-processing* was used to estimate the resolution based on Fourier shell correlation between two independent half-maps. The reconstruction statistics are in Table 2.

2.2. Localized reconstruction of the adenovirus fibre

For the localized reconstruction of the trimeric fibre, we subtracted the signal contributed by the hexons from raw 2D images. To do this, we fitted the asymmetric unit atomic model (PDB:5TX1; all chains except penton base and fibre protein chains N and O) to the icosahedral map and segmented the associated density using the split map function in UCSF Chimera. The extracted density was imported to Scipion and *xmipp3 - create 3d mask* protocol was used to create an icosahedrally symmetric binary mask defining all capsid components except penton bases and trimeric fibres. The mask was used for partial signal subtraction in *relion - subtract projection* protocol to calculate a set of particles lacking these components in the particle projection images (Bai et al., 2015).

To define the twelve fibre sub-particles within each particle image, we used the unit vector [0.000, 0.5257, 0.8507] defining the upper, front-most five-fold vertex for the icosahedrally symmetric reconstruction in the I1 symmetry convention (Supplementary Fig. 3). The sub-particle alignment parameters were calculated using *localrec - define subparticles* protocol using this vector and length of 444 Å, centering the sub-particles in the middle of the penton base. Sub-particle orientations were defined relative to the Z-axis using the 'align subparticles' option. This protocol created 521,040 sub-particles (60 × 8684). Protocol *localrec - filter sub-particles* reduced the number of sub-particles to 69,590 by removing overlapping sub-particles on the five-fold symmetry axes (4 out of 5 for each vertex) and selecting sub-particles located

Table 1
Protocols in Scipion for handling symmetry mismatches.

Software package/plugin	Version	Scipion protocol(s)	Description	References
XMIPP	3.1	*xmipp3 -break symmetry*	Given an input set of particles with angular assignments assigns each particle a symmetry-related orientation randomly	de la Rosa-Trevín et al., 2013
XMIPP	3.1	*xmipp3 -subtract projection*	Subtracts map projections from the experimental particle images	de la Rosa-Trevín et al., 2013
RELION	3.1	*relion -expand symmetry*	Given an input set of particles with angular assignments, for each particle generates all symmetry-related particles	Sjors H. W. Scheres (2012)
LocalRec	2.1	*localrec -define subparticles*	Determines the coordinates, orientations and defocus values of the sub-particles	This study
LocalRec	2.1	*localrec -extract subparticles*	Extracts sub-particle images from each particle image	This study
LocalRec	2.1	*localrec -filter subparticles*	Excludes unwanted sub-particles based on alignment information	This study
LocalRec	2.1	*localrec -stitch subvolumes*	Assembles a full volume from the sub-volumes generated by localized reconstruction	This study
RELION	relax (custom version)	*relion - 3D classification relion - 3D auto-refine*	Relaxes the dominant symmetry by considering multimodal priors centered at the symmetry mates	Ilca et al. (2019)

Table 2
Reconstruction parameters.

	Capsid	Trimeric fibre	Hexon 1	Hexon 2	Hexon 3	Hexon 4
	EMD-11008	EMD-11009	EMD-11010	EMD-11011	EMD-11012	EMD-11013
Pixel size (Å)	1.31	1.31	1.31	1.31	1.31	1.31
Box size (pixels)	1200	140	256	256	256	256
Number of particles	8684	41,638	521,040	521,040	521,040	521,040
Symmetry	I1	C1	C1	C1	C1	C1
Resolution (Å)	3.8/3.9[a]	7.3	3.1	3.1	3.1	3.1
B-factor ($Å^2$)	136	342	111	110	109	109

[a] Local resolution of the hexon 1 in the icosahedral capsid after extracting a box with the same dimensions as the localized reconstructions (256 × 256 × 256).

within 0–40° from the particle side view to exclude those fibres that overlapped significantly with residual capsid and genome density in the projection image. We set the box size to 280 × 280 in *localrec - extract subparticles* protocol to extract sub-particle images from the subtracted particle images. A low-resolution initial volume (10 Å) was calculated using *relion - reconstruct* protocol. A 3D classification focused on the trimeric fibre was then carried out using *relion - 3D classification* protocol to classify the sub-particles into three classes. In order to determine which of the five possible C5-related views of the template matched the observed sub-particle the best, we relaxed the symmetry of the five-fold symmetric penton base (C5) to no symmetry (C1) using our symmetry relaxation by multimodal priors (Ilca et al., 2019) in custom RELION based on version 3.0.6 (available from https://github.com/LSB-Helsinki/relion/tree/ver3.0-relax). For this classification, we used a regularisation parameter T = 4 and no shifts or further rotations were allowed. It is worth mentioning that symmetry relaxation used here is a multimodal prior model since one prior is centered at each symmetry-related orientation of a sub-particle using the option *–relax_sym C5*. A total of 41,638 sub-particles were selected from the class with the majority of sub-particles (57% of total). To calculate two half-maps in addition to the final map at the appropriate resolution in one step, we used *relion - 3D auto-refine* protocol, where no shifts or rotations were allowed (alternatively one could reconstruct the two half-maps and the final map using *relion - reconstruct*). The structure was resolved to 7.6 Å resolution as estimated by FSC (0.143 threshold) using *relion - postprocessing*. The reconstruction statistics are in Table 2.

Atomic model of the fibre knob (PDB:6FJO) was fitted into the localized reconstruction as a rigid body using UCSF Chimera. The fit was performed using the global search function of 'Fit in Map' with 100 random initial placements to prevent any bias. This global fitting was followed by a local optimization to fit the model using cross-correlation metric.

2.3. Reconstruction of the adenovirus capsid from separate sub-particle reconstructions

We reconstructed HAdV-D26 asymmetric unit by combining four localized reconstructions, each centered at one of the four unique hexons that are not related by icosahedral symmetry. Four vectors were defined from the particle centre to the centre point of each hexon protein. The centre point was first calculated by fitting an atomic model of the hexon and calculating its centre of mass in UCSF Chimera. The four vectors were stored as Chimera marker files. Protocol *localrec - define subparticles* was used to calculate the location and orientation of each subparticle in each particle. It is worth noting that, unlike in the case of the trimeric fibre sub-particles (section 2.2), aligning the hexon sub-particles along the Z-axis was unnecessary. A total of 521,040 sub-particles (60 from each particle) for each hexon were extracted from particle images (8,684) pixels using *localrec - extract subparticles* protocol (box size of 256 × 256 pixels). A localized reconstruction was calculated for each hexon using *relion - reconstruct* limiting the resolution to 10 Å. The box size was sufficiently large to include the penton protein in the case of the localized reconstruction of the peripentonal hexon (hexon 1).

To account for potential flexibility of the HAdV-D26 capsids, the four localized reconstructions were further refined by performing a local search around the priors (0.9° initial angular sampling, 1.8° sigma for the angular search range, 1 pixel initial translational sampling, 5 pixel sigma for translational search range) using *relion -*

3D auto-refine protocol. Resolution estimation by FSC and amplitude weighting was carried out using *relion - post-processing* protocol. Because the density of the particle extends outside of the localized reconstruction box, care must be taken to mask the halfmaps with a mask containing a soft edge that reaches zero density value. We created a mask for each low-pass filtered (40 Å) hexon with *relion - create 3D mask* using a threshold of 0.001 and a soft edge (sigma width of 6 pixels). These masks were applied to the halfmaps in the FSC calculation. For an unbiased comparison, a representative volume of the same size (corresponding to hexon 1) was extracted from the icosahedral reconstruction and the FSC was calculated using the same mask and box size. Reconstruction statistics are presented in Table 2. To create a composite model of the capsid, the individual hexon reconstructions were combined using *localrec - stitch subparticles* protocol. The default mask (radius 128 pixels) was used. Icosahedral symmetry was imposed and the composite volume box size of 1200 × 1200 was used.

3. Results

We describe a plugin named LocalRec for the Scipion software framework (de la Rosa-Trevín et al., 2016). The plugin implements the localized reconstruction method we have proposed earlier (Ilca et al., 2015) in addition to new functions which are described in section 3.1. We demonstrate different uses of the LocalRec plugin using previously published cryo-EM images of HAdV-D26 as a test case (Yu et al., 2017). To illustrate integration with standard single particle analysis (SPA) workflows, we first reconstruct the structure of the icosahedrally symmetric capsid of adenovirus (section 3.2). We then use LocalRec to tackle its symmetry-mismatched trimeric fibres (section 3.3) and deviation from icosahedral symmetry (section 3.4) before building a composite model of the entire particle (section 3.5).

3.1. LocalRec plugin for localized reconstruction in Scipion

We chose to implement the method in Scipion for several reasons. First, the Scipion framework has been designed with integration and extensibility at its core. As a result, we could focus on developing new methods and analysis tools, while benefiting from existing functions. Scipion provides developers with many reusable functions and classes for handling and visualizing EM data that facilitate the implementation of new plugins. For instance, since our protocol for defining sub-particles uses the built-in graphical user interface for picking particles, the user can visualize sub-particles within particles as if they were particles within micrographs (Supplementary Fig. 1). Additionally, if in the future new visualization tools are implemented in Scipion, they will be available to our plugin without any extra work. The same applies if new protocols (that produce or consume the same type of data) are integrated from other packages, they could be used together with the protocols provided by the LocalRec plugin. Moreover, Scipion currently provides not only a variety of tools for dealing with symmetry-mismatched structures (Table 1), but also allows to perform higher-order analysis such as examining possible flexibility within subunits. Due to the variety of available tools and the flexibility of the framework, users are never locked into a fixed processing pipeline or a single software package.

The LocalRec plugin includes four protocols: 1. *Localrec - define subparticles* to calculate the coordinates of the sub-particles within each particle and calculate their alignment parameters (section 3.1.1), 2. *Localrec - extract subparticles* to extract sub-particle images from the particle images (section 3.1.2), 3. *Localrec - filter subparticles* to remove sub-particles that are too similar according to certain alignment parameters (section 3.1.3) and 4. *Localrec - stitch subparticles* to build a composite volume from several subvolumes (section 3.1.4). Protocols 1–3 are new implementations of our localized reconstruction method published earlier (Ilca et al., 2015). Protocol 4 is a new addition to LocalRec plugin and analogous to the 'block-based' reconstruction method (Zhu et al., 2018). A typical workflow utilizing these protocols and their integration with standard SPA protocols in the Scipion framework is shown in Fig. 1. In sections 3.1.1, 3.1.2, 3.1.3 and 3.1.4, we describe these protocols and provide guidelines on how to parametrise each protocol.

3.1.1. Defining the sub-particles for each particle

Any structure of interest can have one or more subunits that can be subjected to SPA routines independently of the rest of the complex (Ilca et al., 2015; Huiskonen, 2018). For instance, in adenovirus, a trimeric fibre is bound to each of the twelve pentons located at the icosahedral vertices (Yu et al., 2017). To analyse such subunits, we wrote *localrec - define subparticles* protocol. This protocol uses as inputs the particle alignment parameters, the symmetry of the particle and a vector that specifies the position and view direction of one of the subunits. The vector can be defined in two mutually exclusive ways. First, the terminal point of the vector can be defined as a string [x, y, z] (in angstroms; the initial point of the vector is assumed to be at [0, 0, 0]). If the specified vector is a unit vector (or any other vector with an arbitrary length), the length of the final vector (and thus the coordinates of the terminal point) can be specified with the "Alternative length" parameter in angstroms. Second, one can define the initial and terminal points of the vector in UCSF Chimera by placing two markers on the particle map. The first marker, specifying the initial point, is typically placed at the centre of the particle map and the second marker, specifying the terminal point, is always placed on the sub-structure of interest (Ilca et al., 2015). For improved accuracy, the second marker should be placed at the centre of mass of the substructure, which in turn can be calculated by first fitting an atomic model of the subunit if such a model is available. In either case, these two markers can be saved as a Chimera marker file (CMM) and imported into the protocol instead of giving the vector terminal point coordinates (and alternative length). Irrespective of how the vector has been defined, its initial and terminal point coordinates (Å) are converted to pixels internally in the protocol. We would like to note that the absolute length of the vector itself has no significance as only the direction of the vector and its terminal point coordinates are used to calculate the sub-particle alignment parameters.

The algorithm first multiplies symmetry matrices related to the dominant symmetry group by each particle transformation matrix to generate an intermediate matrix. Euler angles for a sub-particle can be drawn out directly from this intermediate matrix. To calculate shifts, first, the position of the sub-particle within the particle image is calculated by multiplying shift values for x, y, and z (from the last column of the intermediate matrix) by the length of the input vector and adding it to the particle origin coordinates. Then, the decimal parts of x and y values (dec(x) and dec(y)) are considered as sub-particle small shifts relative to the sub-particle origin (originX = −dec(x) and originY = −dec(y)) while the integer parts (int(x) and int(y)) are assigned to the sub-particle coordinate relative to the particle image (coordinateX = int(x) and coordinateY = int(y)). This allows retaining sub-pixel accuracy after extraction of sub-particles from particle images. Sub-particle coordinates of each particle can be visualised using the Scipion particle picker graphical user interface (Supplementary Fig. 1).

To take the defocus gradient across the particle into account, the height of the subunit within the particle (Δz) is subtracted from the defocus value of the particle (z) to get the defocus value of the sub-particle (z'). This is particularly necessary for large complexes such

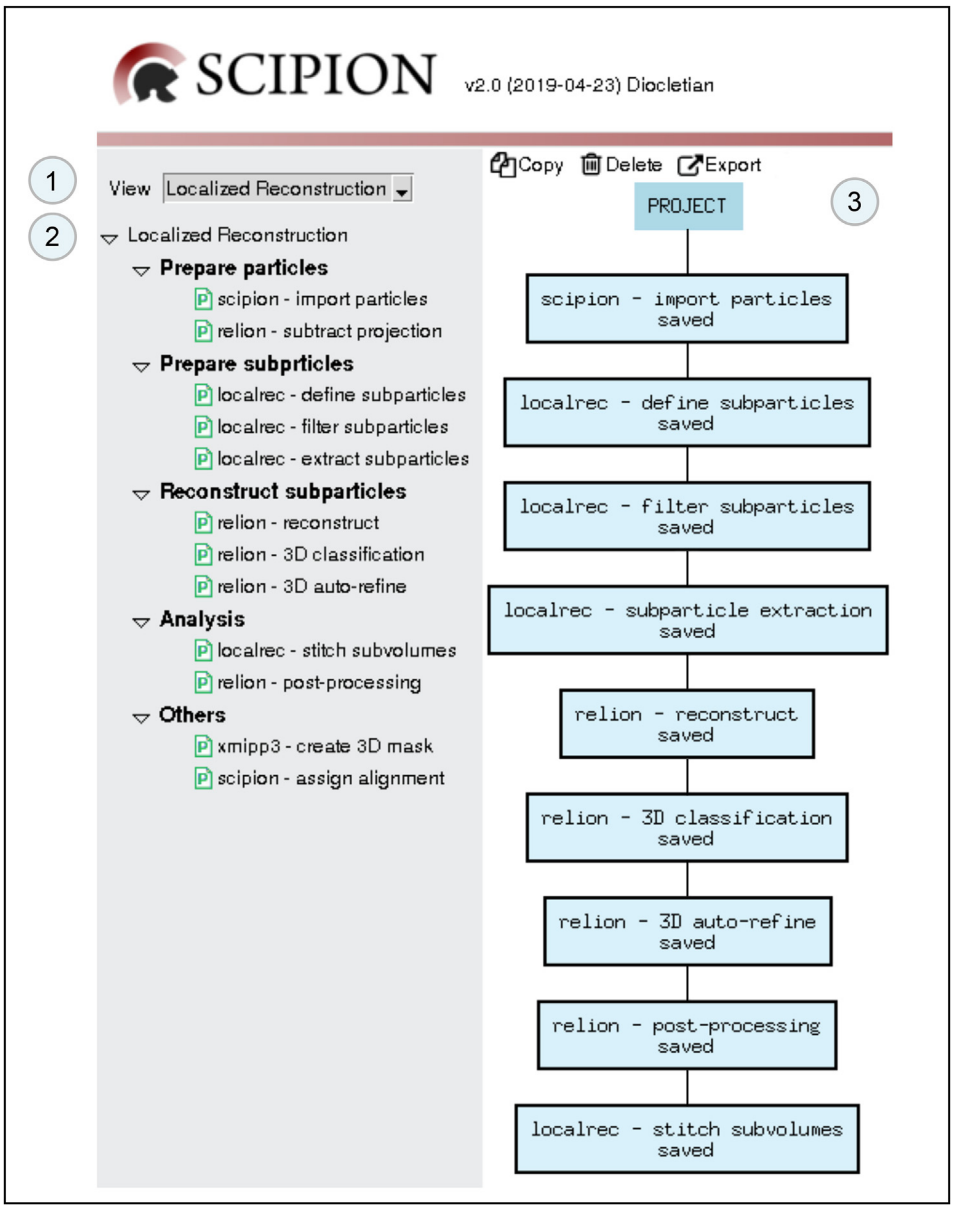

Fig. 1. Localized reconstruction workflow in Scipion. For a list of LocalRec and associated protocols the user can select "Localized Reconstruction" from the dropdown menu (1). The protocols are grouped thematically in the left hand side menu for convenient access (2). A typical Scipion workflow combining several LocalRec and associated protocols (blue boxes) is illustrated (3).

as viruses where the defocus values of the sub-particles coming from the near side and far side of the particle are significantly different from the average defocus value of the particle (DeRosier, 2000; Miyazawa et al., 1999). The effect of this correction is evident for instance when comparing the sub-particle-based density maps calculated for the adenovirus capsid with ($z' = z-\Delta z$) and when the correction is applied in the opposite direction ($z' = z+\Delta z$), a case that would occur if the handedness of the particle reconstruction is inverted relative to the correct handedness (Supplementary Fig. 2).

Two parameters of this protocol require special attention:

1. Align sub-particles: This parameter should be set to 'yes' if the user intends to take possible cyclic symmetry of the subunit into account in the subsequent steps. If set to 'yes', an additional transformation is applied to the particle transformation matrix that brings the original view vector of the sub-particle along the z-axis (standard symmetry convention for cyclic symmetries) and further use of symmetry is possible. If set to 'no', the sub-particles will not be further aligned. Any localized reconstruction of the subunit will then be in the same orientation as the corresponding subunit in the original structure, and further use of the symmetry is not possible. These two alternatives are demonstrated for localized reconstructions of adenovirus penton base–fibre complex (Supplementary Fig. 3).
2. Consider alternative handedness: If set to yes, the opposite hand of the particle reconstruction is assumed to be correct. As a consequence, the defocus gradient correction will be applied in the opposite direction than normally. This allows carrying out localized reconstruction without the need to repeat the reconstruction of the particle to yield a map with correct handedness first. Instead, all maps can be mirrored before starting their

interpretation and building of atomic models. A test using adenovirus capsid localized reconstructions demonstrated that it is important to apply this correction consistently with the particle reconstruction handedness, as the effect is noticeable at the relevant resolution and sample thickness (Supplementary Fig. 2).

3.1.2. Removing sub-particles with overlapping alignment parameters

The defined sub-particles can overlap each other in the projection image of the particle and furthermore they may have overlapping view directions. To illustrate the latter point, we consider the pentons of the adenovirus: icosahedral symmetry produces 60 sub-particles, but if our vector of choice defines the penton base residing on the icosahedral five-fold symmetry axis, we will have 12 sets of 5 sub-particles that differ only in their rotation around the axis. It is often beneficial to filter out such overlapping sub-particles (in our example case to yield only one penton sub-particle per vertex). We wrote *localrec - filter sub-particles* protocol to carry out this task. This protocol provides a set of four filters to exclude sub-particles not intended for further processing based on their alignment parameters. These filters are:

1. Angle to keep unique sub-particles: This filter selects a unique sub-particle within an angular distance which is useful when some sub-particles are on the symmetry axis and when it is not desired to pick such sub-particle several times (e.g., a sub-particle on a five-fold vertex of an icosahedrally symmetric virus). This filter calculates and examines the angle between the view vectors calculated for each pair of sub-particles and discards one of them if the angle is less than this parameter value.
2. Minimum distance between sub-particles: This filter controls the minimum distance between two sub-particles in the particle image to prevent overlapping sub-particles contributing to localized reconstruction. This filter calculates the Euclidean distance between each sub-particle pair in the particle image and rejects all sub-particles within this minimum distance.
3. Angle to keep sub-particles from side views: To select side-view sub-particles within a specified angular distance and discard the rest of the sub-particles. This parameter is useful when top views of sub-particles overlap with other density. A sub-particle will be selected if its view direction is within this angular distance from the side view.
4. Angle to keep sub-particles from top views: Analogously to the previous filter this filter selects those sub-particles that are within the given angular distance from the top view.

3.1.3. Extracting sub-particle images for single-particle analysis

The sub-particles are extracted from the particle images using *localrec - extract subparticles* protocol (Fig. 1). This protocol is similar to the protocols that extract particles from micrographs, such as *xmipp3 - extract particles* and *relion - particles extraction*. As the gray values of the particle image have already been normalized during the extraction of particles from the micrographs, the sub-particles are not further normalized. The only inputs to this protocol are the particle images, the coordinates of the sub-particles and the size of the sub-particle image in pixels. Any sub-particle images that extend outside of the particle image will get discarded. In such cases, and in order to retain these subparticles, the particle images should first be extracted using a larger image box.

It is worth mentioning that the extraction protocol retains the assignment into random half sets. This is crucial, as sub-particles coming from the same particle may have shared pixels due to overlaps and this could lead to overestimation of resolution by FSC. As all the sub-particles coming from a certain particle image inherit the half-set assignment of that particle, they all contribute to the same half-map from localized reconstruction, and this problem can be avoided.

After sub-particle images have been extracted, they can be subjected to common SPA protocols, typically using their alignment parameters as prior information. These include 3D classification (such as *relion - 3D classification*) and 3D refinement (such as *relion - 3D auto-refine*). As part of these protocols, the sub-particles can be subjected to further methods to tackle their conformational heterogeneity (such as *relion - multibody*). These approaches are demonstrated in sections 3.3 and 3.4 on adenovirus fibres and capsid, respectively.

3.1.4. Combining individual sub-particle reconstructions into a composite map

Localized reconstruction of sub-particles creates several separate subvolumes, each representing a subunit or some other local region in the particle. We developed a method for building a composite volume of the particle from its subunits and implemented it as a LocalRec protocol named *localrec - stitch subvolumes* (Fig. 1, Supplementary Fig. 4). The number of input subvolumes is unlimited, so the full volume can be broken into an arbitrary number of subvolumes to capture the inherent flexibility and/or symmetry mismatches among the subunits.

The protocol requires two half-maps for each input subunit from a refinement protocol (e.g. *relion - 3D auto-refine*) and the related vectors defining the position of the subunits relative to the entire particle. These vectors can be read from *localrec - define subparticles* protocols. Supplementary Fig. S4 outlines the different steps of this algorithm. We tested both linear and bilinear interpolation schemes and chose the linear interpolation as default since it is faster and was determined to be accurate enough for this application. This algorithm is computationally expensive since each half-map of each subvolume and the associated mask go through several interpolation steps. To increase computational efficiency, we used Scipion's in-built parallelization strategy to run independent steps simultaneously. For example, the symmetrization of masks and subvolumes are independent tasks and can be performed in parallel as long as there is enough memory available. The protocol outputs two half-maps of the final composite volume, so the user can assess the resolution based on FSC using, for instance, *relion - post-processing* and/or *relion - local resolution* protocols. Alternatively, if the half-maps are not needed, the protocol can be run on the final maps alone to produce a single composite volume. In section 3.5 we demonstrate the use of this protocol on adenovirus.

3.2. Icosahedral reconstruction of human adenovirus serotype 26 in Scipion

To test the developed Scipion protocols, we used hAdV-D26 as subject specimen. We first reconstructed the icosahedrally symmetric structure of the viral capsid using established packages, mainly RELION and related Scipion plugins (see Methods). The density of the capsid was resolved to 3.8 Å resolution (FSC = 0.143 criterion; Supplementary Fig. 5A; Table 2), displaying the features of hexons, pentons and minor proteins consistent with the 3.7 Å resolution reconstruction published earlier (Yu et al., 2017). As expected, the trimeric fibres bound to the penton protein at each of the twelve vertices were not properly resolved due to their flexibility and symmetry-mismatch. This symmetry-mismatch arises from the three-fold symmetry of the trimeric fibre and the five-fold symmetry of the penton protein.

Adenovirus (hAdV-5) capsid has been crystallized and its structure determined to 3.5 Å resolution by X-ray diffraction, suggesting that the structure is relatively rigid (Reddy et al., 2010). However, it is not clear what is limiting the resolution of the X-ray structure and the icosahedral cryo-EM reconstructions to 3.5–3.7 Å resolution. The thickness of the specimen, leading to a defocus gradient across the structure, may limit resolution, but this effect becomes a limiting factor only at resolution 3.0 Å or better (DeRosier, 2000). Thus, we hypothesized that the resolution of the hAdV-D26 capsid in solution may also be limited by flexibility leading to deviations from perfect icosahedral symmetry. Below we demonstrate how the developed LocalRec plugin allows resolving the trimeric fibre (section 3.3), improving the resolution of the capsid (section 3.4) and building a composite map from the different localized reconstructions of capsid subunits and fibres (section 3.5).

3.3. Localized reconstruction of the trimeric adenovirus fibre

Using localized reconstruction in conjunction with symmetry relaxation in RELION (see Methods), we resolved the structure of the trimeric fibre to 7.3 Å resolution (Fig. 2, Supplementary Fig. 6). For this reconstruction, it was beneficial to subtract the contribution of hexons in the images (Bai et al., 2015). Without subtraction, the resolution of the fibre map was lower (8.8 Å; not shown) than with subtraction (7.3 Å). The subtraction also improved the B-factor of the map from 370 Å^2 to 342 Å^2. This suggests that the subtraction improved the alignment and/or classification accuracy of the fibre sub-particles. Although the resolution was limited, presumably due to flexibility or conformational variability, the map at 7.3 Å resolution was of sufficient quality to provide a domain level description of the fibre and allowed fitting of an atomic model. The shaft consists of eight repeats (Fig. 2A) which is in agreement with previous results (Yu et al., 2017). The fibre shows clear three-fold symmetry despite the fact no symmetry was imposed on the map (Fig. 2B, Supplementary Fig. 6B). To further validate the quality of the fibre knob density, we fitted a crystal structure of the HAdV-D26 fibre knob domain (PDB:6FJO; Fig. 2) (Baker et al., 2019). The structure fitted well to the fibre knob density (model-to-map cross correlation 0.94), providing further validation of the reconstruction. Furthermore, we could locate three elbow-shaped fibre N-terminal tails (FNTs) that connect the centre of the fibre to the PB subunits (Fig. 2B). The fiber is tilted ~5° away from the five-fold axis, presumably due to the quasi-equivalent binding modes of the FNTs (Supplementary Fig. 6F).

In conclusion, localized reconstruction and symmetry relaxation allowed resolving the symmetry mismatch in the adenovirus penton, and at least partially dealing with the flexibility of the fibre revealing its tilted conformation. Furthermore, our results confirm the proposed three-pronged fibre claw arrangement for FNTs and the eight-repeat model of the hAdV-D26 fibre shaft.

3.4. Improved reconstruction of the adenovirus capsid

Localized reconstruction of hexons 1–4 yielded maps at 3.1 Å resolution (FSC at 0.143 threshold; see Methods; Fig. 3A; Supplementary Figs. 5B–E; Table 2). For map validation, we fitted the individual HAdV-D26 hexons 1–4 (PDB:5TX1) onto the hexon density maps as rigid bodies. Model-to-map FSCs at 0.5 threshold were 3.4, 3.3, 3.2 and 3.2 Å for hexons 1–4, respectively. Visual examination of the maps and the fitted atomic models showed most side chains agreeing well with the density (a representative area is shown in Supplementary Figs. 5B–E). For comparison, we fitted the hexons 1–4 (PDB:5TX1) to the corresponding hexon densities in the 3.8 Å resolution icosahedral reconstruction yielding map-to-model FSC 3.9, 3.9, 3.8 and 3.8 Å (at 0.5 threshold). Visual comparison of the map quality in the icosahedral reconstruction (Supplementary Fig. 5A) and the hexon localized reconstructions (Supplementary Figs. 5B–E) revealed a comparable level of detail. Some areas were resolved better in the localized reconstructions of the individual hexons than in the icosahedral reconstruction, reflecting the improvement in resolution from 3.8 Å to 3.1 Å in the former.

The localized reconstructions of the hexons (hexon 1 map also containing the PB) were merged together to create a volume for the asymmetric unit (Fig. 3B). Symmetrization of this volume yielded a composite map of the entire adenovirus capsid (Fig. 3C). This composite map is comparable to the conventional icosahedral reconstruction but benefits from the improved resolution for the hexons (Supplementary Fig. 6).

In conclusion, the developed localized reconstruction protocols are accurate and able to resolve high-resolution detail. Furthermore, calculating a composite model of the capsid using the four hexon localized reconstructions allowed building a complete density map of the capsid. All maps created by the LocalRec protocol provided a similar or higher level of detail compared to conventional icosahedral reconstruction.

3.5. Composite model of the adenovirus virion

A composite model of the entire HAdV-D26 particle consisting of the capsid with twelve fibres was generated from hexons and trimer fibre localized reconstructions (Fig. 4). Applying symmetry on the trimeric fibre poses a challenge. Icosahedral symmetry of the capsid corresponds to 60 symmetry operators, however only 12 trimeric fibres bind each capsid. Applying these operators on the fibre localized reconstruction would result in an average of five fibre densities at each five-fold symmetric vertex of the capsid. To tackle this, we defined a subset of the symmetry operators, corresponding to one fibre per vertex (Fig. 4A). It is worth noting that for any given HAdV-D26 particle image, alignment parameters were determined here only for a subset of its fibre sub-particles (as those fibre sub-particles that overlapped with the rest of the particle were excluded from alignment). In theory, the number of different types of possible HAdV-D26 particles, when it comes to their fibre orientations, is very large (5^{12} including those related by symmetry). Here, for the purpose of creating one model and for simplicity, the symmetry operator for each five-fold vertex was chosen randomly. Combining the twelve fibres with the capsid composite model (Fig. 4B) allowed creating a representative composite model of the HAdV-D26 particle (Fig. 4C). In conclusion, this approach allowed combining the high-resolution structure of the capsid subunits with the lower resolution map of the fibre with its correct symmetry.

4. Discussion

Many symmetrical biological complexes contain additional subunits that do not follow the dominant symmetry. In such complexes, imposing the dominant symmetry averages out the symmetry-mismatched subunits. In the last few years, cryo-EM packages have started to include increasingly sophisticated tools for asymmetric single-particle image analysis (Huiskonen, 2018; Goetschius et al., 2019). The stand-alone Python implementation of localized reconstruction (Ilca et al., 2015) and its derivatives have been used in several studies such as determining the structure of flexible clathrin cages (Morris et al., 2019), classifying different dsRNA genome organisations in a virus capsid (Ilca et al., 2019), estimating the occupancy of receptor KREMEN1 bound to coxsackie virus A10 (Zhao et al., 2020), as well as tackling the asymmetric

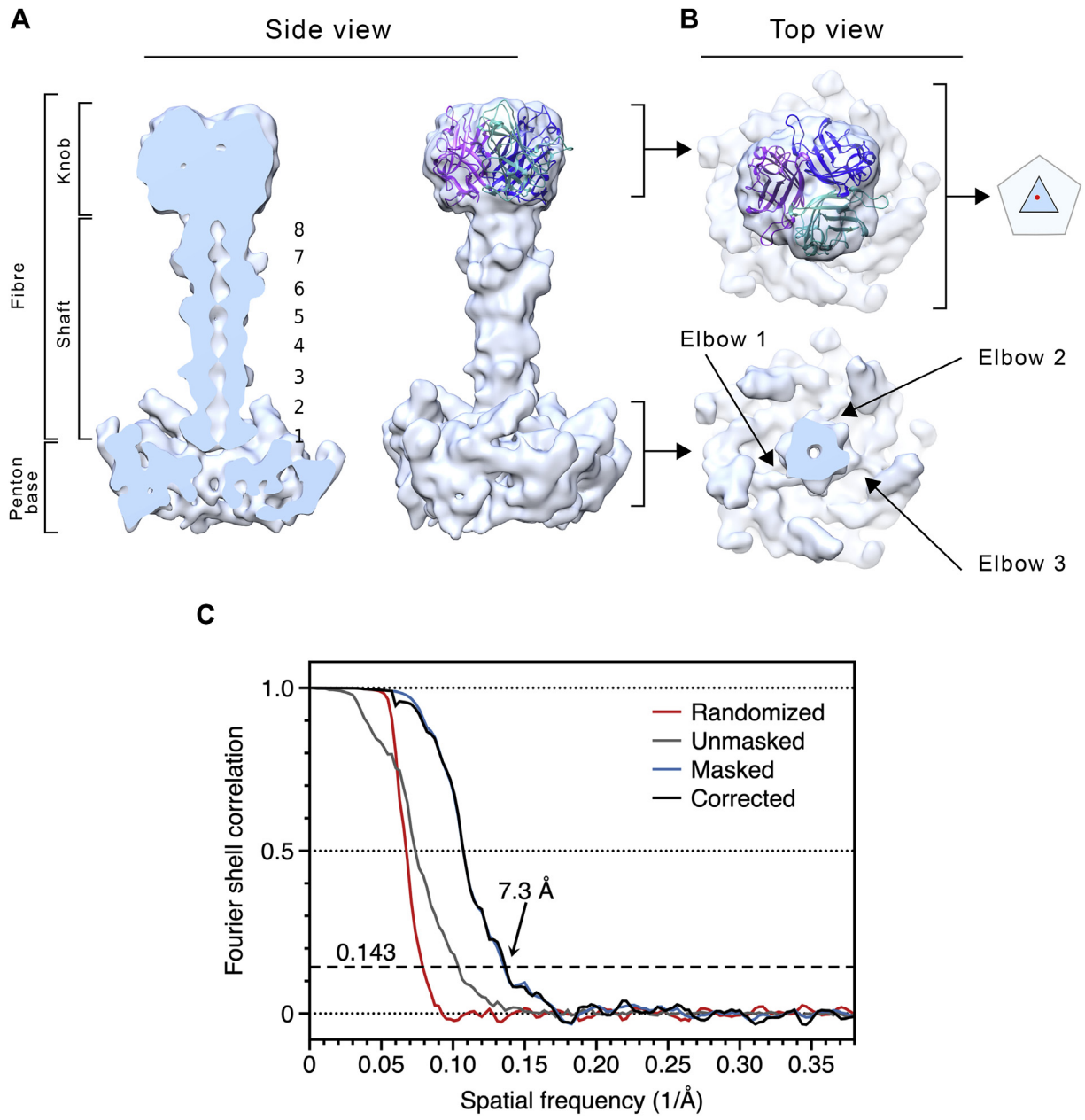

Fig. 2. Localized reconstruction of the adenovirus penton. (A) A localized reconstruction of the trimeric fibre bound to the underlying penton base is shown from the side as a cut-open (left) and complete (right) surface model. The former surface model shows several cavities (1–8) likely corresponding to the eight repeating structural motifs proposed to make the shaft region. The latter surface model shows an atomic model of the knob region (PDB:6FJO) fitted into the density as a rigid body. The model is rendered as ribbon and the different subunits of the trimer are colored blue, teal and purple. (B) Top view of the fibre, cut at different heights (as shown in *A*), shows the knob region (top) and the shaft–penton base contact region (bottom). The schematic diagram illustrates how the three-fold symmetric fibre (triangle) is shifted relative to the centre point (red dot) of the five-fold symmetric penton base (pentagon). The bottom panel shows the three elbow-like densities (elbow 1–3) connecting the fibre to the penton base. Two of them (elbow 1 and 2) bind to neighboring penton subunits and the third (elbow 3) is distal to the first two. (C) Resolution assessment of the penton by Fourier shell correlation. The effect of masking (Masked) was tested by phase randomisation (Randomized; starting at 1/18.3 Å spatial frequency and dropping to zero as expected) to yield the final corrected FSC curve (Corrected). The resolution at which this curve intersects the threshold (dashed line at 0.143) is indicated.

binding of prefoldin to TRiC/CCT chaperonin (Gestaut et al., 2019), the flexibility-induced blurring of Tra1 within the chromatin modifying complex SAGA (Sharov et al., 2017) and the "variable domains" of translation initiation factor eIF2 (Adomavicius et al., 2019).

Here, we wrote a plugin named LocalRec to include the localized reconstruction method in the Scipion software framework, to extend its functionality and to improve its accuracy. The plugin was implemented using mainly Scipion core functions and avoiding dependencies to other software packages, thus facilitating streamlined updates of the code in the future.

We used the LocalRec plugin to determine the structure of HAdV-D26 trimeric fibre to 7.3 Å resolution. The same structure has been studied earlier using localized reconstruction (Yu et al., 2017). In contrast to our density map of the fibre, in the earlier structure, the knob density did not show clear three-fold symmetry and two extra, artificial FNT densities were visible in addition to the three true FNT densities. This suggests that the earlier methods used to determine the orientation of the spike were suboptimal, leaving many fibre sub-particles misaligned. Here the LocalRec plugin

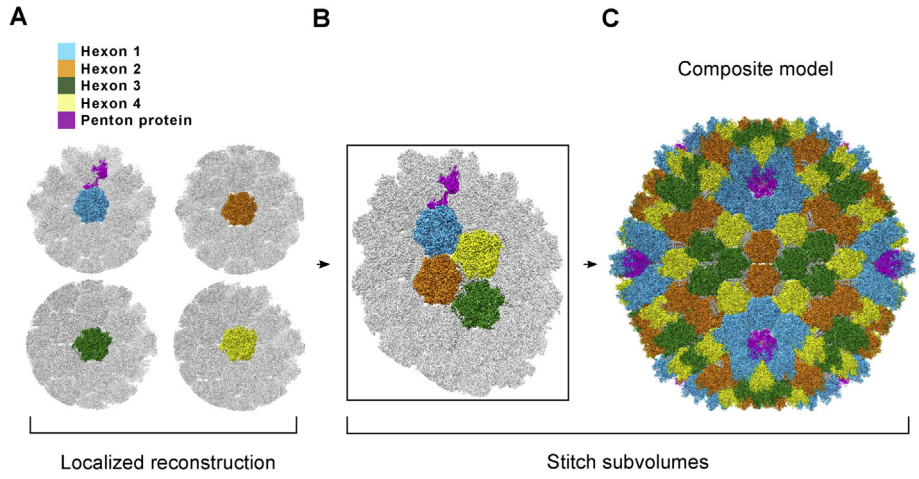

Fig. 3. Localized reconstructions of adenovirus capsid subunits. (A) Localized reconstructions of the four hexons forming the asymmetric unit. Each map has a part of density for neighboring hexons. Hexon 1 (cyan) also includes the penton protein (purple). (B) Composite model of the asymmetric unit calculated by combining individual hexon localized reconstructions in panel *A*. (C) Composite model of the full adenovirus capsid after applying icosahedral symmetry on the asymmetric unit in panel *B*.

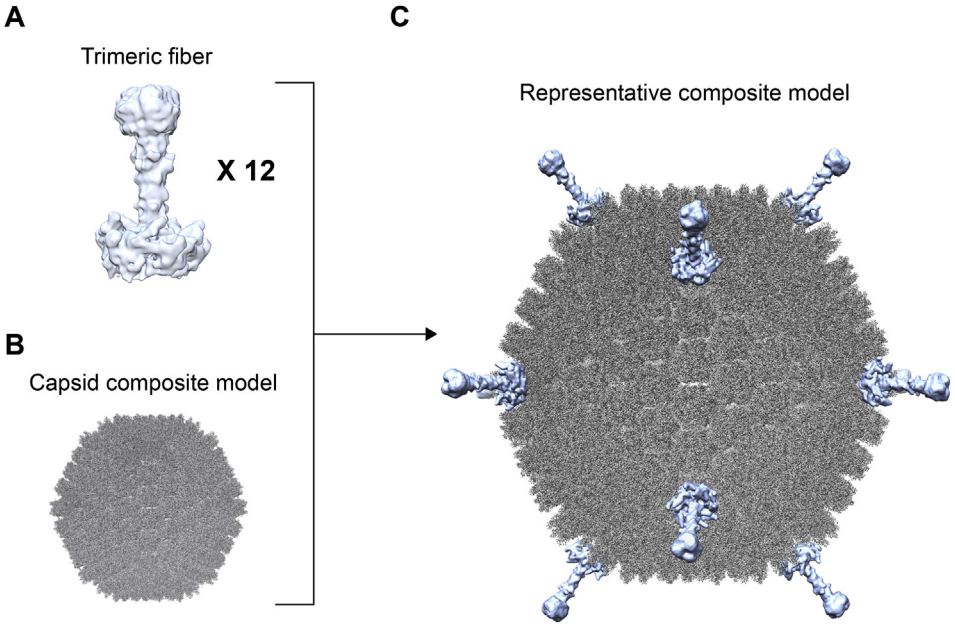

Fig. 4. Composite model of the adenovirus virion. (A) Application of twelve transformations on the localized reconstruction of the fibre. (B) Masked reconstruction of the capsid with hexons and pentons. (C) A composite model created by overlaying the twelve fibres and the capsid map.

together with the symmetry relaxation we implemented in RELION allowed determining the three-fold features of the trimeric fibre.

The alignment of individual building blocks separately, followed by stitching them back together, allows both correcting for flexibility and the defocus gradient, which is especially critical for large structures such as viruses. Earlier this method has been used for instance to improve the resolution of herpes simplex virus 1 capsid from 4.2 Å to 3.5 Å (Dai and Zhou, 2018). Further alignment of capsid building blocks may be especially useful in resolving structures with noticeable quasi-symmetry, where the subunits deviate significantly from their ideal positions (Huiskonen, 2018). For instance, both sindbis virus (Chen et al., 2018) and Rift Valley fever virus (Halldorsson et al., 2018) show significant conformational flexibility in the outer glycoprotein shell and localized reconstruction has been employed to improve the resolution of the capsomers. In such cases, the asymmetric unit can be divided into as many sub-particles as is required to deal with deviations from perfect symmetry. After aligning the sub-particles, the entire particle can now be built from its sub-particle localized reconstructions. Here the adenovirus capsid, a fairly rigid structure, provided a control case to demonstrate the accuracy of the implemented protocols.

5. Conclusion

The localized reconstruction method has previously been demonstrated to be useful in a wide variety of cases (Halldorsson et al., 2018; Morris et al., 2019; Ilca et al., 2019; Gestaut et al., 2019; Pang et al., 2019; Sharov et al., 2017; Zhao et al., 2020). The development of LocalRec plugin for Scipion, a common and well-established software framework (de la Rosa-Trevín et al., 2016), is expected to facilitate further adaptation and development of this

method. By seamless integration to all existing single particle methods available in Scipion, LocalRec will expedite investigations of biomolecular mechanisms that often involve symmetry-mismatched components, flexible subunits and transient interactions.

Author contributions

Wrote the LocalRec plugin and further developed symmetry relaxation for RELION (V.A.). Performed the initial integration of localized reconstruction to Scipion (S.L.I., J.G-B., J.M.d.l.R-T). Provided supervision (J-M.C., J.T.H.). Provided data (V.R.). Analysed the data (V.A., I.R., J.T.H.). Wrote the manuscript (V.A., J.T.H.). All authors read and commented on the final manuscript.

CRediT authorship contribution statement

Vahid Abrishami: Software, Methodology, Investigation, Validation, Visualization, Writing - original draft. **Serban L. Ilca:** Software, Validation, Writing - review & editing. **Josue Gomez-Blanco:** Software. **Ilona Rissanen:** Visualization, Writing - review & editing. **José Miguel de la Rosa-Trevín:** Software, Supervision, Writing - review & editing. **Vijay S. Reddy:** Resources, Writing - review & editing. **José-Maria Carazo:** Supervision, Funding acquisition. **Juha T. Huiskonen:** Conceptualization, Funding acquisition, Writing - original draft, Supervision, Project administration.

Declaration of competing interest

The authors declare no competing interests.

Acknowledgments

This project was funded by European Research Council under the European Union's Horizon 2020 research and innovation programme (649053 to J.T.H.) and by a Wellcome Trust four-year PhD studentship (109135/Z/15/A to S.L.I.). Work in the laboratory of J.T.H. is funded by the Helsinki Institute of Life Science HiLIFE. This work benefited from access to the Instruct-ERIC centre Electron Microscopy Image Processing I2PC, Madrid, Spain. Financial support was provided by Instruct-ERIC (PID 1772). The authors wish to acknowledge CSC — IT Centre for Science, Finland, for computational resources.

Appendix A. Supplementary data

Supplementary data to this article can be found online at https://doi.org/10.1016/j.pbiomolbio.2020.05.004.

References

Adomavicius, T., Guaita, M., Zhou, Y., Jennings, M.D., Latif, Z., Roseman, A.M., Pavitt, G.D., 2019. The structural basis of translational control by eIF2 phosphorylation. Nat. Commun. 10 (1), 2136. https://doi.org/10.1038/s41467-019-10167-3.

Bai, X.C., Rajendra, E., Yang, G., Shi, Y., Scheres, S.H., 2015. Sampling the conformational space of the catalytic subunit of human γ-secretase. eLife 4 (e11182). https://doi.org/10.7554/eLife.11182.

Baker, A.T., Mundy, R.M., Davies, J.A., Rizkallah, P.J., Parker, A.L., 2019. Human adenovirus type 26 uses sialic acid-bearing glycans as a primary cell entry receptor. Science Advances 5 (9), eaax3567. https://doi.org/10.1126/sciadv.aax3567.

Chen, L., Wang, M., Zhu, D., Sun, Z., Ma, J., Wang, J., Kong, L., et al., 2018. Implication for alphavirus host-cell entry and assembly indicated by a 3.5Å resolution cryo-EM structure. Nat. Commun. 9 (1), 5326. https://doi.org/10.1038/s41467-018-07704-x.

Dai, X., Zhou, Z.H., 2018. Structure of the herpes simplex virus 1 capsid with associated tegument protein complexes. Science 360 (6384). https://doi.org/10.1126/science.aao7298.

de la Rosa-Trevín, J.M., Otón, J., Marabini, R., Zaldívar, A., Vargas, J., Carazo, J.M., Sorzano, C.O., 2013. Xmipp 3.0: an improved software suite for image processing in electron microscopy. J. Struct. Biol. 184 (2), 321–328. https://doi.org/10.1016/j.jsb.2013.09.015.

de la Rosa-Trevín, J.M., Quintana, A., del Cano, L., Zaldívar, A., Foche, I., Gutiérrez, J., et al., 2016b. Scipion: a software framework toward integration, reproducibility and validation in 3D electron microscopy. J. Struct. Biol. 195 (1), 93–99. https://doi.org/10.1016/j.jsb.2016.04.010.

DeRosier, D.J., 2000. Correction of high-resolution data for curvature of the Ewald sphere. Ultramicroscopy 81 (2), 83–98. https://doi.org/10.1016/s0304-3991(99)00120-5.

Gestaut, D., Roh, S.H., Ma, B., Pintilie, G., Joachimiak, L.A., Leitner, A., Walzthoeni, T., Aebersold, R., Chiu, W., Frydman, J., 2019. The chaperonin TRiC/CCT associates with prefoldin through a conserved electrostatic interface essential for cellular proteostasis. Cell 177 (3), 751–765. https://doi.org/10.1016/j.cell.2019.03.012 e15.

Goetschius, D.J., Lee, H., Hafenstein, S., 2019. CryoEM reconstruction approaches to resolve asymmetric features. Adv. Virus Res. 105, 73–91. https://doi.org/10.1016/bs.aivir.2019.07.007.

Grigorieff, N., 2016. Frealign: an exploratory tool for single-particle cryo-EM. Methods Enzymol. 579, 191–226. https://doi.org/10.1016/bs.mie.2016.04.013.

Guo, F., Liu, Z., Vago, F., Ren, Y., Wu, W., Wright, E.T., Serwer, P., Jiang, W., 2013. Visualization of uncorrelated, tandem symmetry mismatches in the internal genome packaging apparatus of bacteriophage T7. Proc. Natl. Acad. Sci. U.S.A. 110 (17), 6811–6816. https://doi.org/10.1073/pnas.1215563110.

Halldorsson, S., Li, S., Li, M., Harlos, K., Bowden, T.A., Huiskonen, J.T., 2018. Shielding and activation of a viral membrane fusion protein. Nat. Commun. 9 (1), 349. https://doi.org/10.1038/s41467-017-02789-2.

Huiskonen, J.T., 2018. Image processing for cryogenic transmission electron microscopy of symmetry-mismatched complexes. Biosci. Rep. 38 (2) https://doi.org/10.1042/BSR20170203. BSR20170203.

Ilca, S.L., Kotecha, A., Sun, X., Poranen, M.M., Stuart, D.I., Huiskonen, J.T., 2015. Localized reconstruction of subunits from electron cryomicroscopy images of macromolecular complexes. Nat. Commun. 6 (Nov 4), 8843. https://doi.org/10.1038/ncomms9843.

Ilca, S.L., Sun, X., El Omari, K., Kotecha, A., de Haas, F., DiMaio, F., Grimes, J.M., Stuart, D.I., Poranen, M.M., Huiskonen, J.T., 2019. Multiple liquid crystalline geometries of highly compacted nucleic acid in a dsRNA virus. Nature 570 (7760), 252–256. https://doi.org/10.1038/s41586-019-1229-9.

Miyazawa, A., Fujiyoshi, Y., Stowell, M., Unwin, N., 1999. Nicotinic acetylcholine receptor at 4.6 A resolution: transverse tunnels in the channel wall. J. Mol. Biol. 288 (4), 765–786. https://doi.org/10.1006/jmbi.1999.2721.

Morais, M.C., Tao, Y., Olson, N.H., Grimes, S., Jardine, P.J., Anderson, D.L., Baker, T.S., Rossmann, M.G., 2001. Cryoelectron-microscopy image reconstruction of symmetry mismatches in bacteriophage phi29. J. Struct. Biol. 135 (1), 38–46. https://doi.org/10.1006/jsbi.2001.4379.

Morris, K.L., Jones, J.R., Halebian, M., Wu, S., Baker, M., Armache, J.P., Avila Ibarra, A., et al., 2019. Cryo-EM of multiple cage architectures reveals a universal mode of clathrin self-assembly. Nat. Struct. Mol. Biol. 26 (10), 890–898. https://doi.org/10.1038/s41594-019-0292-0.

Nakane, T., Kimanius, D., Lindahl, E., Scheres, S.H., 2018. Characterisation of molecular motions in cryo-EM single-particle data by multi-body refinement in RELION. eLife 7 (Jun 1), e36861. https://doi.org/10.7554/eLife.36861.

Pang, S.S., Bayly-Jones, C., Radjainia, M., Spicer, B.A., Law, R.H.P., Hodel, A.W., Parsons, E.S., et al., 2019. The cryo-EM structure of the acid activatable pore-forming immune effector macrophage-expressed gene 1. Nat. Commun. 10 (1), 4288. https://doi.org/10.1038/s41467-019-12279-2.

Reddy, V.S., Natchiar, S.K., Stewart, P.L., Nemerow, G.R., 2010. Crystal structure of human adenovirus at 3.5 A resolution. Science 329 (5995), 1071–1075. https://doi.org/10.1126/science.1187292.

Rohou, A., Grigorieff, N., 2015. CTFFIND4: fast and accurate defocus estimation from electron micrographs. J. Struct. Biol. 192 (2), 216–221. https://doi.org/10.1016/j.jsb.2015.08.008.

Scheres, S.H., 2016. Processing of structurally heterogeneous cryo-EM data in RELION. Methods Enzymol. 579, 125–157. https://doi.org/10.1016/bs.mie.2016.04.012.

Scheres, S.H., 2012. A bayesian view on cryo-EM structure determination. J. Mol. Biol. 415 (2), 406–418. https://doi.org/10.1016/j.jmb.2011.11.010.

Sharov, G., Voltz, K., Durand, A., Kolesnikova, O., Papai, G., Myasnikov, A.G., Dejaegere, A., Ben Shem, A., Schultz, P., 2017. Structure of the transcription activator target Tra1 within the chromatin modifying complex SAGA. Nat. Commun. 8 (1), 1556. https://doi.org/10.1038/s41467-017-01564-7.

Yu, X., Veesler, D., Campbell, M.G., Barry, M.E., Asturias, F.J., Barry, M.A., Reddy, V.S., 2017. Cryo-EM structure of human adenovirus D26 reveals the conservation of structural organization among human adenoviruses. Science Advances 3 (5), e1602670. https://doi.org/10.1126/sciadv.1602670.

Zhao, Y., Zhou, D., Ni, T., Karia, D., Kotecha, A., Wang, X., Rao, Z., et al., 2020. Hand-foot-and-mouth disease virus receptor KREMEN1 binds the canyon of coxsackie virus A10. Nat. Commun. 11 (1), 38. https://doi.org/10.1038/s41467-019-13936-2.

Zhu, D., Wang, X., Fang, Q., Van Etten, J.L., Rossmann, M.G., Rao, Z., Zhang, X., 2018. Pushing the resolution limit by correcting the ewald sphere effect in single-particle cryo-EM reconstructions. Nat. Commun. 9 (1), 1552. https://doi.org/10.1038/s41467-018-04051-9.